mater.scichina.com link.springer.com

Published online 14 March 2022 | https://doi.org/10.1007/s40843-021-1977-5
Sci China Mater 2022, 65(8): 2252–2261

SPECIAL ISSUE: Flexible Intelligent Materials

Highly stretchable and self-healable ionogels with multiple sensitivity towards compression, strain and moisture for skin-inspired ionic sensors

Yufeng Wang[1], Ying Liu[1], Nan Hu[1], Peiru Shi[1], Chao Zhang[1*] and Tianxi Liu[1,2*]

ABSTRACT **Ionic skin (I-skin) is an emerging skin-inspired sensor that has received increasing interest for the next-generation wearable electronics. However, profound challenges for I-skin remain in achieving multiple signal responses (e.g., strain, pressure, and humidity) and self-healability to fully mimic human skin. Herein, a Fe^{3+} ion-coordinated poly(acrylic acid) ionogel (PAIFe) with high stretchability, extreme temperature tolerance, and self-healing capability is prepared by a dynamic ionic cross-linking strategy. The ionic coordination in the PAIFe contributes to the formation of a highly dynamic network, achieving its high-efficient and reliable self-healing performance even at a low temperature of −20°C. Using of 1-butyl-3-methylimidazolium tetrafluoroborate ([BMIm][BF_4]) as the solvent achieves a wide-temperature tolerance of the PAIFe under low and high temperatures. More interestingly, a humidity sensing function is realized in the PAIFe by skillfully utilizing the hygroscopic properties of [BMIm][BF_4]. The resultant PAIFe is proof-of-concept demonstrated as a deformation-tolerant ionic conductor in a skin-inspired ionic sensor, showing a variety of sensory capabilities towards compression, strain and humidity.**

Keywords: stretchable ionic conductor, ion coordination, dynamic cross-linking, self-healability at low temperature, skin-inspired sensor

INTRODUCTION

Artificial skin aims to intelligently imitate various perceptual abilities of strain, pressure and humidity from the external environments by mimicking human skin [1–3], showing great potential in wearable electronics, soft robotics and health monitoring [4,5]. Ionic conductive hydrogel, a kind of soft material with the integration of high stretchability, ionic conductivity, transparency, biocompatibility and adaptability [6–11], meets the demand of artificial skin for flexible wearable fearures and has gained much interest in the emerging field of ionic skin (I-skin) [12]. Ideal materials for the I-skin are expected to have the ability to perceive a variety of stimuli and adapt to complex environments to meet the needs of comprehensively simulating the perception functions of human skin [13–15]. However, hydrogels have to use water as the solvent, facing the problem of instability in a hot or cold environment [16]. High temperature causes dehydration, while low temperature causes freezing of hydrogels, eventually resulting in the loss of physical properties and functions of devices. Furthermore, hydrogels confine a large amount of water in polymer networks, reducing its ability to perceive humidity, which dramatically limits its simultaneous sensing capability of multiple types of stimuli [17,18]. Among the various sensing capabilities of I-skin, the sensing ability of moisture is more challenging to be realized than that of strain or pressure [19]. Therefore, the realization of the stimuli-responsive and environment-stable ionic conductors in respond to multiple types of stimuli is of great need for the development of the emerging I-skin.

Ionogel is a soft material with a three-dimensional polymer network confining ionic liquids (ILs) [20–22]. Ionogel combines the characteristics of hydrogels and ILs, not only having excellent ionic conductivity, thermal stability and chemical inertness but also having high mechanical elasticity, thus showing great prospects in the field of I-skin [23]. However, for the application in I-skin, most existing ionogels have the problems of poor mechanical properties, such as the irreversible recovery at large strain and the low fracture energy [24–26]. In addition, I-skin needs to withstand the complex and changeable applied environments [27,28], such as large deformation and continuous mechanical loading in a variety of temperatures and humidities, which inevitably lead to structural damages and device failures. The self-healing ability provides a new feature that significantly increases the reliability, lifetime and safety of devices [29–31]. Although self-healing ionogels have been reported, these materials are often difficult to self-heal at low temperatures [32], and the self-healing process usually requires external stimulations (e.g., light, heat) [33–35]. Therefore, the development of ionogels with autonomous healing at a low temperature and excellent mechanical elasticity is urgently needed for the new-generation I-skin, while meets challenges.

Herein, a dynamic ionic cross-linking strategy is presented for preparing an Fe^{3+} ion-coordinated poly(acrylic acid) ionogel (PAIFe) by using an IL of 1-butyl-3-methylimidazolium tetrafluoroborate ([BMIm][BF_4]) as the solvent. Due to the high

[1] State Key Laboratory for Modification of Chemical Fibers and Polymer Materials, College of Materials Science and Engineering, Donghua University, Shanghai 201620, China
[2] Key Laboratory of Synthetic and Biological Colloids, Ministry of Education, School of Chemical and Material Engineering, Jiangnan University, Wuxi 214122, China
* Corresponding authors (emails: czhang@dhu.edu.cn (Zhang C); txliu@jiangnan.edu.cn (Liu T))

thermal stability and low vapor pressure of [BMIm][BF_4], the as-obtained PAIFe shows highly stable mechanical and ionic conductive performance under an extremely wide temperature range from −60 to 80°C. The Fe^{3+} ion-coordination endows the PAIFe with not only high elasticity but also low-temperature yet high-efficient self-healability. Notably, even at the low temperature of −20°C, the PAIFe exhibits a favorable self-healability with a high healing efficiency of 87%. Importantly, as a typical hygroscopic IL, the [BMIm][BF_4] is capable of spontaneously absorbing and releasing moisture from the surrounding environment. As a result, the PAIFe with the balanced water contents under a variety of humidity environments shows distinguishably different resistances, making the PAIFe promising to detect environmental humidity. A skin-inspired ionic sensor was proof-of-concept fabricated, demonstrating high sensitivity in monitoring ambient humidity, as well as human physiological signals of joint bending, pressing and breathing. The dynamic ionic cross-linking ionogels with multiple responsibilities have great prospects in the design of multifunctional I-skin for detecting multi-modal signals.

EXPERIMENTAL SECTION

Materials

Acrylic acid (AA, >98%), [BMIm][BF_4], 1-ethyl-3-methylimidazolium dicyanamide ([EMIM][$N(CN)_2$]) and 1-butyl-3-methylimidazolium bis(trifluoromethylsulfonyl)imide ([BMIM][TFSI]) were obtained from Adamas. Ferric nitrate nonahydrate ($Fe(NO_3)_3{\cdot}9H_2O$) was obtained from Sinopharm Chemicals. Diethoxyacetophenone (photoinitiator, 95%) was obtained from TCI. Deionized (DI) water was used in the experiments.

Preparation of PAIFe

In a typical procedure, 1 g of AA and 40 mg of $Fe(NO_3)_3{\cdot}9H_2O$ were completely dissolved in 4 g of [BMIm][BF_4], and then 50 mg of diethoxyacetophenone was added to the above solution under stirring in a nitrogen atmosphere. The mixed solution was cast into a square poly(tetrafluoroethylene) (PTFE) mold (20 mm × 5 mm × 2 mm) and subsequently cured under ultraviolet (UV) light (CL-1000L, λ: 365 nm, power: 8 W) for 1 h. The cured sample was transferred into an oven at 40°C for another 12 h to complete the polymerization. Finally, the ionogel sample was kept in a constant humidity box (relative humidity (RH): 30%, 20°C) for 48 h, producing the PAIFe-2. For comparison, the PAIFe-1 and PAIFe-3 were prepared by placing the resultant samples in a constant humidity box at the RH value of 10% and 80%, respectively, while maintaining all other conditions same as the PAIFe-2. Samples of polyacrylic acid (PAA) hydrogels (PAH) cross-linked by Fe^{3+} ions (PAHFe) were prepared according to the similar method but with the addition of water instead of [BMIm][BF_4] in the same weight.

Characterization

Fourier transform infrared (FT-IR) spectra were recorded on a Nicolet 8700 spectrometer using an attenuated total reflectance (ATR) method in the range of 4000–400 cm^{-1}. Rheological measurements of ionigel samples were recorded on a rheometer (Anton Paar, MCR 302) using a 25 mm diameter parallel plate. Amplitude-sweep rheological tests were measured at a fixed frequency of 10 rad s^{-1} at a shear strain range from 0.1% to 1000%. Alternate step amplitude-sweep tests were recorded at an alternating 1% and 700% shear strains five times under a frequency of 10 rad s^{-1}. Frequency-sweep rheological measurements were performed at a frequency range from 1 to 100 rad s^{-1} at a 1% shear strain. Temperature-frequency sweep tests were measured at a frequency range from 1 to 100 rad s^{-1} at a 1% shear strain in a temperature range of 0.1 to 80°C. Tensile measurements (samples in the sizes of 10 mm × 5 mm × 2 mm) were tested on a universal testing machine (SUNS, UTM2102). All samples were tested at room temperature with a tensile rate of 30 mm min^{-1}. Dynamic mechanical analysis (DMA) measurements were tested on a dynamic mechanical analyzer (DMA 1, METTLER). Measurements were set at a fixed frequency (1 Hz) and strain (0.1%) and recorded under a heating rate of 10°C min^{-1} at a temperature range from −90 to 50°C. The self-healing process of samples was observed on an optical microscope (BX-51, Olympus). Ionic conductivity of ionogel samples (samples in the sizes of 5 mm× 5 mm × 2 mm) was recorded on an electrochemical station (CHI 660E) and calculated from Equation (1):

$$\sigma = L / (R \times S), \quad (1)$$

where σ, S, L and R are the conductivity, cross-sectional area, thickness and charge transfer resistance of ionogel samples, respectively.

Measurements of skin-inspired ionic sensors

The skin-inspired ionic sensor was integrated by two pieces of ionogel samples (sample sizes of 10 mm × 5 mm × 2 mm), a dielectric elastomer (3M 4905) and three current collectors. Force sensing performance of the sensor was recorded on an LCR meter (TH2832) at a sweeping frequency of 1 kHz and an alternating current (AC) voltage of 1 V. The resistance signals were recorded on a source meter (Keithley 2616) at a voltage of 3 V. A home-made humidity-controlled system was used to provide various RH conditions by a bubbling method. Specifically, wet air was produced by bubbling the dry air through the water. The various RH conditions were obtained by mixing the dry air with the wet air in a designed volume proportion while keeping the total air pressure at 0.1 MPa. Prior to the testing, the PAIFe-2 sensor was purged with an accurately proportioned gas flow (the ratio of dry air to wet air at 7:3) for 300 s. The PAIFe-2 sensor for detecting the surrounding environments at a variety of RH values was achieved by blowing the gas with different RH values on the surface of sensor. The sensor could return to the initial state by blowing another accurately proportioned gas (the ratio of dry air to wet air at 7:3) surrounding the sensor. During the testing, it was assumed that the PAIFe-2 sensor could reach the balance under the designed RH values when the resistances of the device changed slowly (resistance changes less than 2% within 5 s).

RESULTS AND DISCUSSION

Fig. 1 illustrates the preparation procedure of the PAIFe. A representative PAIFe sample was prepared through a one-pot UV-photopolymerization of the precursor solution containing AA, $Fe(NO_3)_3{\cdot}9H_2O$, [BMIm][BF_4] and the photoinitiator at room temperature. Physical cross-linking of the PAIFe with the interactions of hydrogen bonds from the adjacent PAA chains and the ionic coordination between Fe^{3+} and $-COO^-$ in PAA were achieved during the *in-situ* polymerization. In virtue of the combination of the hydrophilic polymeric network of PAA and the hygroscopic liquid medium of [BMIm][BF_4], the PAIFe is

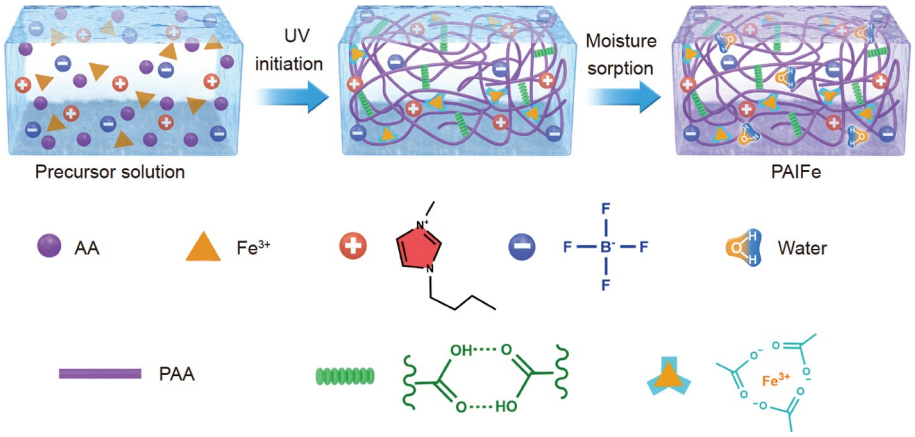

Figure 1 Schematic illustration of the design principle and fabrication of the PAIFe.

highly sensitive to moisture. The prepared PAIFe samples are marked as the PAIFe-1, PAIFe-2 and PAIFe-3 when the as-polymerized PAIFe samples were stored in a humidity chamber at an RH of 10%, 30% and 80%, respectively, at 20°C for 48 h. Water contents of the PAIFe-1, PAIFe-2 and PAIFe-3 were measured and shown in Fig. S1. The results demonstrate their water contents following the order of PAIFe-1 < PAIFe-2 < PAIFe-3, which suggests that the water contents of the PAIFe increase with the increase of environmental humidity during their preparations. Ionic conductivity of the PAIFe samples was measured and compared in Fig. S1. The results show that the ionic conductivity increases with the increased water content in the PAIFe samples, which is attributed to the water contents boosting the ion migration and decreasing the overall resistance of the resultant PAIFe. Ionic conductivities of the PAIFe using different kinds of ionic liquids as solvents were investigated in Fig. S2. The results show that the PAIFe using the [BMIm][BF_4] as the solvent exhibits relatively large conductivity changes compared with the PAIFe samples using the [BMIm][TFSI] and [EMIm][$N(CN)_2$] as the solvents. When the RH values increase from 20% to 60%, the relative resistance changes increase dramatically amomg the PAIFe-2, suggesting the optimized humidity sensing performance by using the [BMIm][BF_4] as the solvent within the ionogels. Furthermore, compared with that of the PAIFe using the [BMIm][TFSI] and [EMIm][$N(CN)_2$] as solvents, respectively, the PAIFe using the [BMIm][BF_4] as the solvent has a relatively high ionic conductivity at the low temperature of −30°C, which is attributed to the anti-freezing property of [BMIm][BF_4] with a relatively low melting point (Fig. S2). It is worthy mentioning that the PAIFe is capable of being shaped into various shapes, like the heart, flower, seahorse and starfish (Fig. S3). Fig. S4 shows that the PAIFe is capable of being stretched to a 300% strain and instantaneously recovered to its initial shape when releasing the external force, indicating its excellent mechanical stretchability and reversibility.

The interactions between the polymer network and the solvent in the PAIFe were explored by the FT-IR spectroscopy. Fig. 2a shows that the characteristic peak of the freeze-dried PAHFe at 1696 cm^{-1} corresponds to the stretching vibration of the C=O groups [36,37]. The FT-IR spectra of the PAIFe samples have distinct peaks at around 1575 and 1060 cm^{-1}, corresponding to the imidazole ring skeleton and the B–F stretching vibration in the [BMIm][BF_4], respectively. The peak of C=O shifts from 1696 cm^{-1} of the freeze-dried PAA to 1708 cm^{-1} of the PAIFe-1, indicating the formation of hydrogen bonds between the [BMIm][BF_4] and PAA. The broad peak from 3300 to 3600 cm^{-1} corresponds to the –OH groups of water. Furthermore, the intensity of the –OH peak gradually increases when the PAIFe was stored in a relatively high humidity environment, which is attributed to a hygroscopic process of the PAIFe. The results suggest that the PAIFe is capable of regulating the environmental humidity spontaneously.

The tensile stress-strain curves were tested to investigate the effects of humidity on the mechanical properties of the PAIFe samples (Fig. 2b). The PAIFe-1 exhibits a high fracture strength (654 kPa) and an elastic modulus (1.51 MPa) but a low elongation at break (65%). When the PAIFe was placed in a relatively high humidity environment that caused the increase of water contents in the PAIFe, the elastic modulus and stretchability of the PAIFe changed in a wide range (Fig. 2c). When there are low contents of water in the PAIFe, the formation of dense hydrogen bonds between the side chain of PAA leads to a high elastic modulus and low elongation at break. Upon the addition of water, the elastic modulus of the PAIFe decreases accompanied by the increase of tensile ductility, which is attributed to the introduction of water as a small molecule plasticizer reducing the hydrogen-bonded interactions between the PAA side chains. The results show that the PAIFe-2 exhibits an optimal mechanical performance in toughness (104.4 kJ m^{-3}) and tensile strength (365.1 kPa). Successive stretching/releasing tensile tests were conducted in a tensile strain range from 50% to 300% (Fig. S5). The results show that the PAIFe-2 has a negligible plastic deformation (15%) even at the large tensile strain of 300%, indicating its good recovery ability.

The mechanical behaviors of the PAIFe samples were further explored by rheological tests. The amplitude-sweep rheological tests were used to define the linear viscoelastic region of the PAIFe samples. The results show that the loss moduli (G'') of all PAIFe samples are lower than their storage moduli (G') at a small shear strain (<10%), which is attributed to the negligible deformation damages of the PAIFe structures and the elastic responses to the deformation (Fig. S6) [38,39]. The G'' values are higher than their G' values at a large shear strain, indicating that the solid-like elastic structures in the PAIFe were damaged and translated into viscous fluids. Furthermore, the PAIFe-1 shows a lower transition point (defined by the value of $G' = G''$) than those of PAIFe-2 and PAIFe-3 at an increased shear strain, suggesting the cross-linking structures of PAIFe-1 are easily

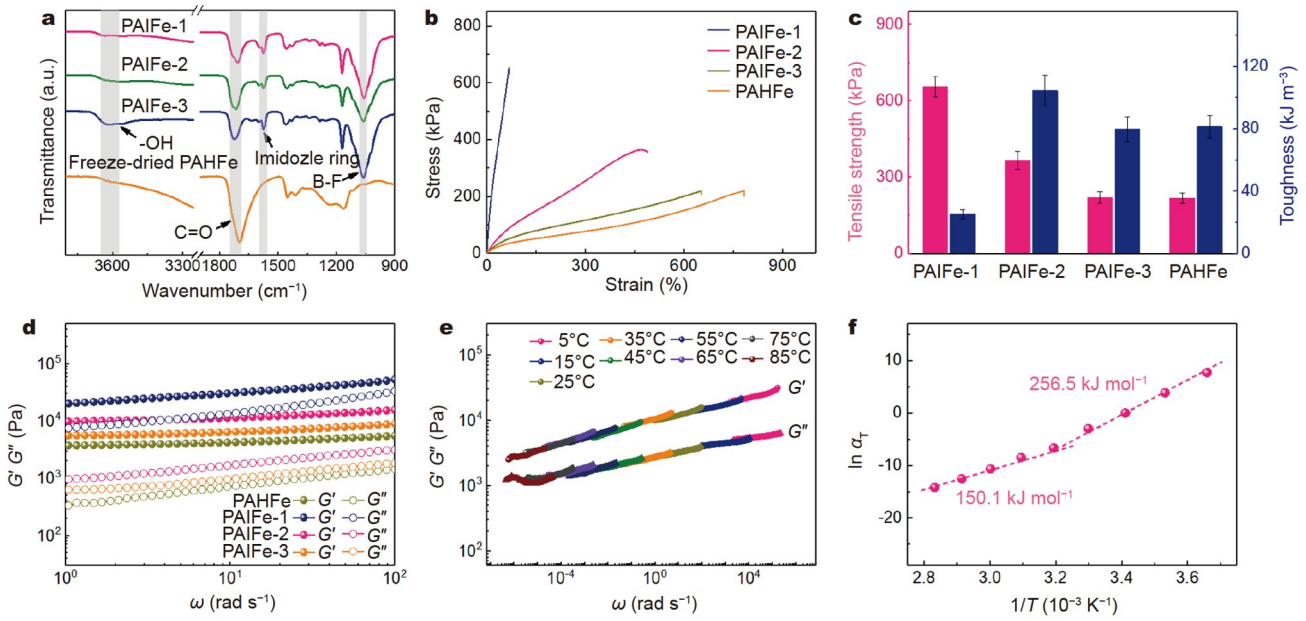

Figure 2 Characterization of the PAIFe with physically cross-linked networks. (a) FT-IR spectra of freeze-dried PAHFe and PAIFe. (b) Typical tensile stress-strain curves of PAHFe and PAIFe. (c) Tensile strength and toughness of PAHFe and PAIFe. (d) Frequency sweep measurements of PAHFe and PAIFe in the angular frequency range from 1 to 100 rad s^{-1}. (e) Frequency dependence of the storage modulus G' and loss modulus G'' of PAIFe-2. (f) Activation energy of PAIFe-2 derived from the Arrhenius plot.

damaged under large deformation. The frequency-sweep rheological measurements show that the G' values of PAIFe-1 are higher than those of PAIFe-2 and PAIFe-3 in the whole frequency range, which further suggests that the PAIFe-1 has a more dense cross-linked network (Fig. 2d). To further systematically investigate the dynamic cross-linked network in the PAIFe, the frequency-sweep rheological tests were conducted at different temperatures (constructed by nine group temperatures of 0.1, 10, 20, 30, 40, 50, 60, 70 and 80°C, respectively) with frequencies from 1 to 100 rad s^{-1}. The master curve of the PAIFe-2 was recorded and processed at the reference temperature of 20°C based on a time-temperature superposition (Fig. 2e). In addition, the frequency-scale shift factor (a_T) of the PAIFe-2 was calculated and evaluated by the separate curves measured at various temperatures. As a result, the Arrhenius plot was generated by the apparent activation energy at different temperatures based on the Arrhenius equation ($a_T = Ae^{E_a/RT}$), where E_a is the apparent activation energy, R is the ideal gas constant and A is a constant. The Arrhenius plot of the PAIFe-2 exhibits two apparent activation energy values with a high and low E_a of 256.5 and 150.1 kJ mol^{-1} (Fig. 2f), respectively. This result suggests that there exist two kinds of physical cross-linking structures with various bonding strengths in the PAIFe-2, which are assigned to the physical interactions of strong ionic coordination interactions and weak hydrogen-bonded interactions, respectively. The strong and weak physical dual-cross-linking structures are in good explanation to the mechanical properties with high tensile strength and large toughness in the PAIFe-2. The strong physical network enhances the mechanical strength, while the abundant hydrogen bonds effectively dissipate the tensile energy.

An excellent temperature-tolerant feature of the PAIFe at both high and low temperatures is achieved and explored in Fig. 3. The PAIFe-2 exhibits high mechanical flexibility that endures the stretching at 100% even at a low temperature of −50°C and the twisting at a high temperature of 60°C (Fig. 3a, b). For comparison, the PAHFe loses its mechanical flexibility after being stored at the same temperature and storing time (Fig. S7a, b). The extremely temperature-tolerant feature of the PAIFe is attributed to the unique characteristics of the [BMIm][BF_4] with low volatility and low freezing point. To further investigate the extreme temperature-tolerant feature, the mass losses of the PAIFe and PAHFe at 80°C and room temperature were measured, respectively. At room temperature (RH range: 40% to 70%), the PAIFe-2 and PAIFe-3 exhibit negligible mass losses, and PAIFe-1 exhibits a slight mass increase after 20 days, which shows the self-adaptive performance of PAIFe to the surrounding environment (Fig. 3c). However, the PAHFe loses most of its moisture after 3 days under the similar conditions. Even at the temperature of 80°C, the PAIFe exhibits a negligible mass loss, while the PAHFe loses almost all its moisture after 10 h (Fig. S8). Weight retentions of the PAIFe at a variety of RH values were also measured. Fig. S9 shows that the PAIFe-2 exhibits a negligible mass loss at a low humidity (RH: 20%, 25°C) within 48 h, and the mass of the PAIFe-2 increases slightly at a 60% RH. The DMA measurements of the PAIFe and PAHFe were conducted in the temperature range of −90 to 50°C (Fig. 3d and Fig. S10). Fig. 3d shows that the values of G' and G'' of the PAIFe-2 keep steady when the temperature is above −66°C. Until the temperature continues to drop, the values of G' and G'' increase rapidly, indicating that the PAIFe-2 begins to change from the elastic state to the glassy state. For comparison, the values of G' and G'' of the PAHFe increase rapidly when the temperature drops to −6°C, which is ascribed to the freezing of water in the hydrogel network and the PAHFe changing from the elastic state to the glassy state (Fig. S10). The results also demonstrate that the PAIFe-2 maintains its mechanical flex-

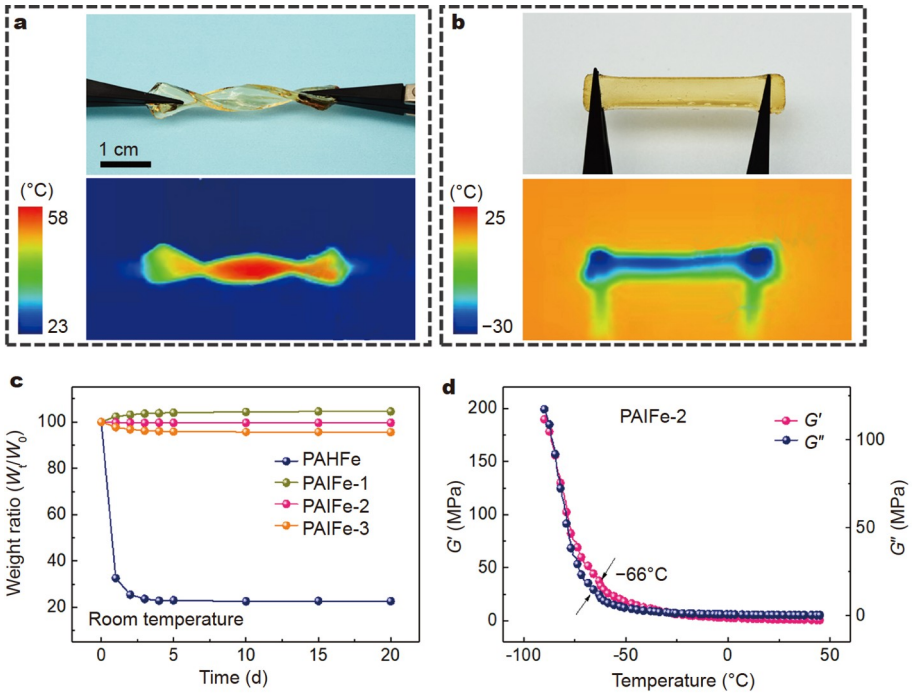

Figure 3 Temperature tolerance of the PAIFe. Infrared images and digital photos of PAIFe that is (a) twisted at 60°C and (b) stretched at −50°C. (c) Weight retention of PAHFe and PAIFe as a function of time at room temperature. (d) DMA measurements of PAIFe-2.

ibility in a wider temperature range than PAHFe, which effectively resists changing to fragile when the PAIFe-2 is in the hot or cold environments.

Self-healability is a promising feature of improving the reliability, lifetime and safety of devices, which is usually constructed by the reorganization of dynamic bonds. Due to the formation of reversible and dynamic hydrogen bonds and ionic coordination interactions, the PAIFe-2 exhibits excellent self-healability both in the conductive and mechanical performance. Fig. 4a exhibits that two cut PAIFe-2 segments are capable of healing in 12 h, and the healed PAIFe-2 can be stretched without damaging the healed crack, indicating reliable self-healability in mechanical performance. Fig. 4b records the whole self-healing process of the PAIFe-2 by a time-dependent optical micrograph at room temperature. The crack at the damaged interface of the PAIFe-2 gradually decreases and disappears within 12 h, which suggests the macrostructure of PAIFe-2 has been self-healed. Mechanical properties and self-healing performance of the PAIFe with various Fe^{3+} ion contents were explored. Fig. S11 shows that the elastic modulus of the PAIFe increases with the increased ferric ion contents. When the mass ratio of PAA to Fe^{3+} ion is set at 20/1, the PAIFe shows an optimized elongation at break (637%) and fracture mechanical strength (287 kPa). In addition, the PAIFe at this PAA/Fe^{3+} ion ratio also exhibits a high self-healing efficiency of ~97%, which is due to the coordination interaction with an appropriate strength at the ratio of PAA and Fe^{3+} ions. The tensile stress-strain curves show that the mechanical performance of the PAIFe-2 is nearly restored to the original value with a 96% healing efficiency (defined by the area under the stress-strain curve) after self-healing for 24 h at room temperature (Fig. 4c). Interestingly, the PAIFe-2 also shows reliable self-healability at a low temperature. After healing for 24 h at a temperature of −20°C, the healing efficiency of PAIFe-2 reaches 87%. The excellent self-healability of PAIFe-2 at the low temperature is derived from the dynamic cross-linked network and the high mobility of the molecular chains at such low temperatures. The [BMIm][BF_4] and a certain amount of water in the PAIFe-2 reduce the hydrogen-bonded interactions between the PAA side chains and provide an anti-freezing feature, which can achieve high molecular chain mobility at a low temperature. The dynamic cross-linked structures from the hydrogen bonds and ionic coordination interactions effectively reconfigure the network structures when the PAIFe-2 is damaged. Even when the PAIFe was cut and self-healed for three cycles, the PAIFe shows the self-healing efficiency up to 91% compared with its original mechanical performance based on the fracture energy calculated from the tensile stress-strain curves (Fig. S12).

Importantly, the healing time of damaged PAIFe-2 could be shortened with the assistance of heating. Fig. S13 shows the mechanical properties of damaged PAIFe-2 repaired in 1 h at a temperature of 60°C, which is attributed to the acceleration of the dynamic-bond recombination by thermal stimulation. In addition to excellent mechanical self-healability, the PAIFe-2 shows reliable self-healability in electrical performance. Fig. 4d shows the electrical recovery of the PAIFe-2 upon a cutting/healing cycle. The complete PAIFe-2 depicts a minimal resistance, indicating its excellent electrical conductivity. The resistance value of the PAIFe-2 increased rapidly and exceeded the instrument limits when the PAIFe-2 was cut into two halves. The resistance was restored to the original value when two segments of the PAIFe-2 were fused. This behavior was repeated twice, revealing the excellent electrical recovery capability of the PAIFe-2. Fig. S14 shows that the ionic conductivity of the PAIFe could recover to 98% of its initial value. Fig. S15 shows a complete circuit composed of the healed PAIFe-2 as a conductor. The blue light emitting diode (LED) indicator was successfully lighted under a 5 V driving voltage. Moreover, the healed PAIFe-2 is capable of being stretched immediately, and

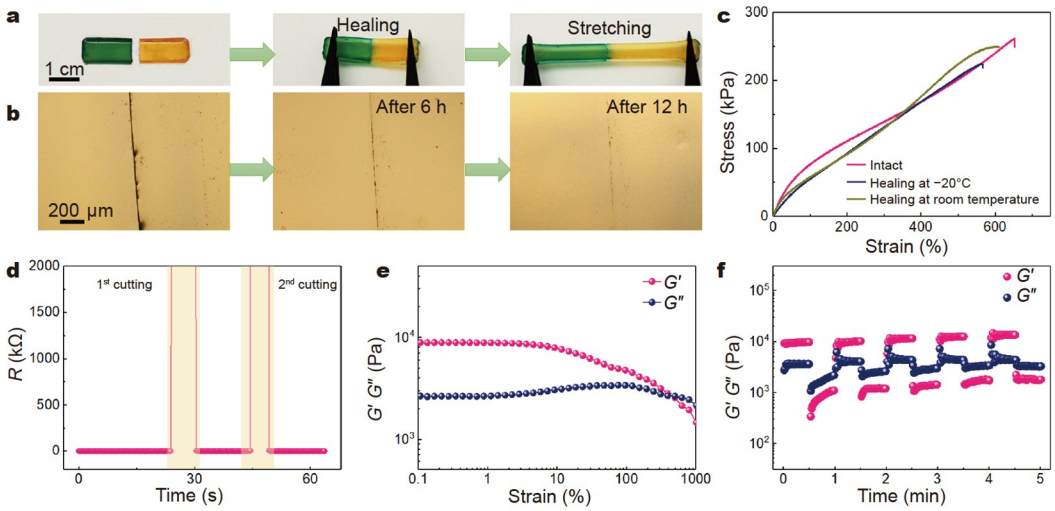

Figure 4 Self-healing performance of the PAIFe. (a) Digital photos of PAIFe-2 after cutting and self-healing processes. (b) Time-dependent optical microscope images of PAIFe-2 upon cutting. (c) Tensile stress-strain curves of PAIFe-2 and damaged PAIFe-2 that was healed at different temperatures. (d) Resistance changes of PAIFe-2 before fracture and after self-healing. (e) Rheological strain sweeping measurement of PAIFe-2 from the strain of 0.1% to 1000%. (f) Continuous step-strain sweep measurement of PAIFe-2 with alternating shear strains of 1% and 700%, repsectively.

the LED indicator is not extinguished, further indicating the excellent self-healability in both the electrical and mechanical performance.

The self-healability of PAIFe-2 was further explored by rheological tests. The amplitude-sweep tests show that the G' values are higher than the G'' values at a small shear strain (<10%, like an elastic solid), and the G' value intersects with the G'' value at the ~500% shear strain, indicating that the PAIFe-2 converts to a quasi-liquid state (Fig. 4e). The step amplitude-sweep measurements with alternate small (1%) and large (700%) shear strains (30 s at each stage) were tested to determine the deformation recovery performance of the PAIFe-2 (Fig. 4f). At the first stage with the shear strain of 1%, the G' values are higher than the G'' values, while the G' values are lower than the G'' values at the second stage (shear strain of 700%), suggesting that the cross-linked networks of PAIFe-2 are damaged at a large shear strain. Surprisingly, when the shear strain returns to 1%, the G' and G'' values recover instantaneously to the initial states, suggesting the damaged structures are repaired in a short time. The alternate small (1%) and large (700%) shear strains were repeated five times and the results suggest the recovery of the PAIFe-2 is repeatable with a similar efficiency.

The intriguing properties of the PAIFe-2 ionic conductor with hygroscopicity, high stretchability and self-healability show great potential for multifunctional skin-inspired sensors. A multifunctional sensor was integrated by two pieces of PAIFe-2, a dielectric elastomer and three current collectors (Fig. 5a). The upper PAIFe-2 monitors the resistance changes between current collectors 1 and 2 caused by moisture. Compared with the humidity and temperature, the capacitive sensors show significantly high sensitivity to the mechanical stimulation (e.g., pressure and strain). According to the capacitance calculation equation, $C = \varepsilon S/4\pi kd$ (S, ε, k and d are the effective area of the two pieces of the electrodes, the dielectric constant, the electrostatic constant and the thickness, respectively), the changes of the thickness or the effective area of the two pieces of electrodes result in the capacitive changes. Therefore, the skin-inspired sensor is capable of detecting external compression and tension. The capacitance of the whole sensor can be accessed from the current collectors 1 and 3.

Fig. 5b shows the real-time responses of the PAIFe-2 skin-inspired sensor to the stretching-releasing process with various deformations by using the capacitance signals. With the increase of tensile strain, the capacitance signals of the device increase, which is attributed to the rise in the effective area of the two pieces of the PAIFe-2 and the decrease in the thickness of the dielectric elastomer. Moreover, the PAIFe-2 sensor well repeats the responses three times in each strain, reflecting a reliable monitoring performance. To simulate the actual monitoring process, the PAIFe-2 sensor was tested at different loading speeds. The results show a highly repeatable and stable capacitive response at the frequency ranging from 0.05 to 0.2 Hz with a 50% tensile strain (Fig. 5c), suggesting that the PAIFe-2 sensor is almost unaffected by the applied frequency. The mechanical stimulation of compressive sensing performance was also measured for the PAIFe-2 sensor. Fig. 5d shows that the PAIFe-2 sensor is capable of detecting various compressive stresses, indicating a high selectivity in a wide compressive stress range.

Unlike the existing ionic conductive hydrogel-based sensors, the PAIFe-2 skin-inspired sensor exhibits excellent humidity-sensing performance. This unique performance comes from the hygroscopicity of ionic liquids, i.e., [BMIm][BF_4] can spontaneously absorb/release moisture from the surrounding environment, which changes the overall resistance of the PAIFe-2, making it possible to detect the humidity. Fig. 5e shows the real-time humidity-sensing performance of the PAIFe-2 sensor at various RH values of 40%, 60%, 80% and 95% by using the resistance signals. With the increase of the applied RH values, the resistance signals of the device increase (e.g., to a relatively small resistance value). For comparison, the device fabricated by the PAHFe shows almost no responses under each RH value, which is attributed to a large amount of water in the polymer network reducing the response to humidity. Furthermore, the PAIFe-2 sensor exhibits a stable humidity-sensing performance even after being stored for 100 days (Fig. 5f). This excellent durable performance is due to the stable environmental stability

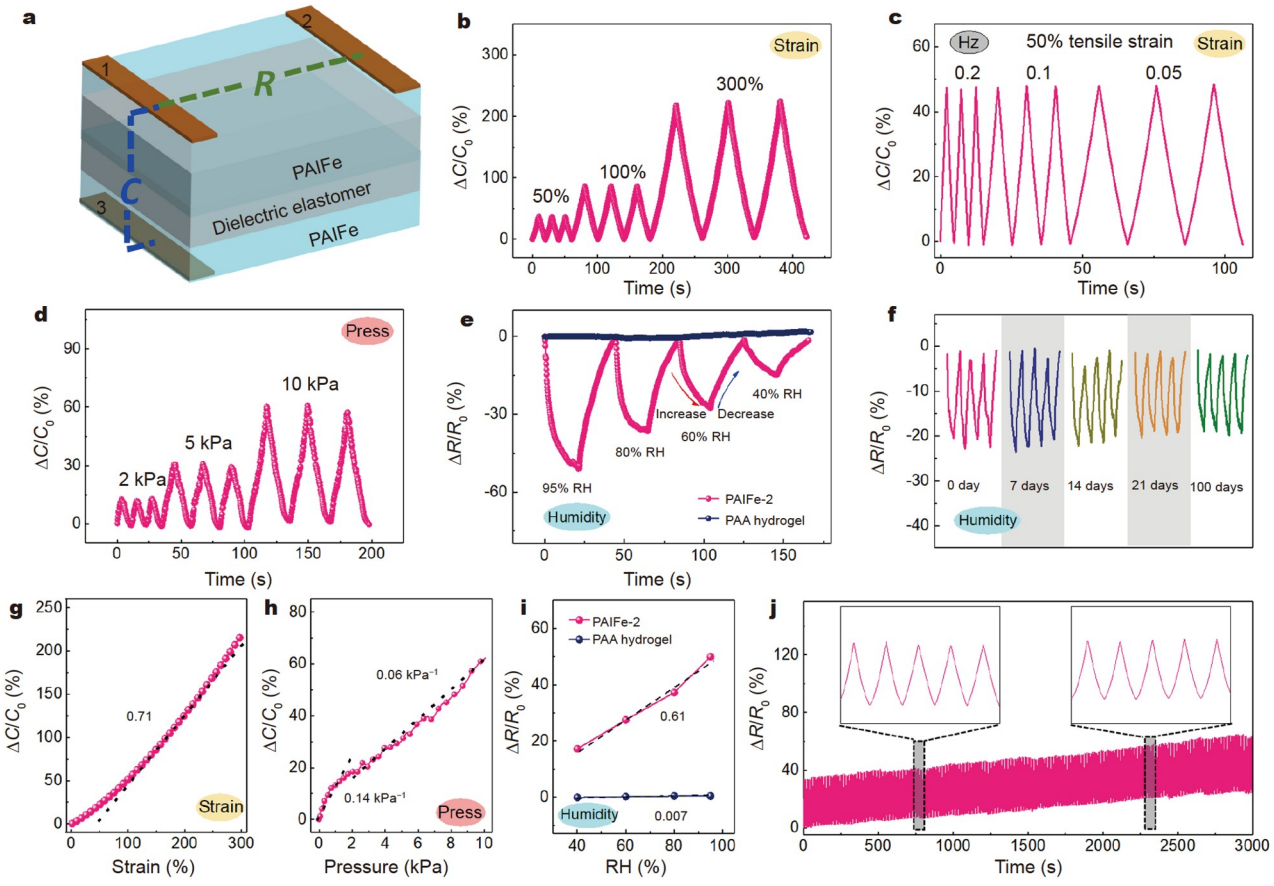

Figure 5 Performance of integrated skin-inspired sensory system. (a) Schematic illustration of the structure of skin-inspired sensors. Relative capacitance variations of the PAIFe-2 sensor in response to various (b) tensile strains, (c) loading frequencies, and (d) applied pressures. (e) Relative resistance variations of the PAIFe-2 and PAHFe sensors in response to various RH environments. (f) Relative resistance variations of the PAIFe-2 sensor in response to RH 60% after storing at room temperature for different days. Sensitivity of the PAIFe-2 sensor to various stimuli of (g) strain, (h) pressure and (i) humidity. (j) Cycling stability of the PAIFe-2 sensor. Inset of (j) showing the relative capacitance variations from 750 to 800 and 2250 to 2300 s, respectively.

of the PAIFe-2.

Fig. 5g–i evaluate the sensitivity of the PAIFe-2 sensor to various stimulus signals. The results show that the PAIFe-2 sensor displays a linear relationship between the tensile strain (0–300%) and capacitance. The gauge factor (GF, GF = $(C - C_0)/(eC_0)$, where e is the tensile strain) was used to evaluate the strain sensing performance, and the GF value of the PAIFe-2 sensor is 0.71 in the strain range of 0 to 300% (Fig. 5g). The PAIFe-2 sensor clearly shows two distinct linear capacitance segments according to different compression pressures (Fig. 5h). The pressure sensing performance of the PAIFe-2 sensor was evaluated by the sensitivity ($S = (C - C_0)/(PC_0)$, where P is the applied pressure). For the PAIFe-2 sensor, the calculated sensitivity is 0.14 kPa^{-1} in the first segment (at a low-pressure range of 0–1 kPa). A sensitivity of 0.06 kPa^{-1} is observed in the second segment (at a high-pressure range of 1–10 kPa). The relatively low sensitivity of the PAIFe-2 sensor at high pressures is attributed to the excessive deformation resulting in the constraint of ion shuttle distance. For the humidity-sensing performance, a relatively linear relationship between the RH value and resistance signal is observed (Fig. 5i), confirming the Langmuir adsorption isotherm model. In addition to the sensitivity, fatigue resistance is a vital quality for a sensor. Fig. 5j shows the PAIFe-2 sensor exhibits high durability in 3000 loading/unloading cycles at a constant tensile strain. The magnified view obviously exhibits that the capacitive response keeps at a stable amplitude and waveform, further suggesting the high reliability.

As a demonstration, the PAIFe-2 sensor can serve as a multifunctional I-skin for multimodal detections (strain, pressure and humidity). Fig. 6a shows the as-assembled PAIFe-2 sensor for monitoring the finger bending at different angles of 30°, 60° and 90°. The amplitudes of capacitance signals correspond with the various bending angles. With the increase of bending angles, the sensor deforms drastically, resulting in an enhancement in the capacitance signals. Fig. S16a, b show that the PAIFe-2 sensor is also capable of detecting the movements of the elbow and knee. The PAIFe-2 sensor can also be used to monitor the pressure from the finger (Fig. 6b). The PAIFe-2 sensor exhibits excellent response and repeatability to both low and high pressures. The PAIFe-2 sensor can also be used to monitor human breathing, by using its response to the humidity. The resistance value of the PAIFe-2 sensor responds instantly to the changes in ambient humidity that is induced by breathing (Fig. 6c). Fig. S17 shows that the PAIFe-2 sensor exhibits the reliable humidity monitoring performance of detecting human breathing under various deformations (e.g., stretching, bending, and twisting), suggesting the negligible influence during deformations. These

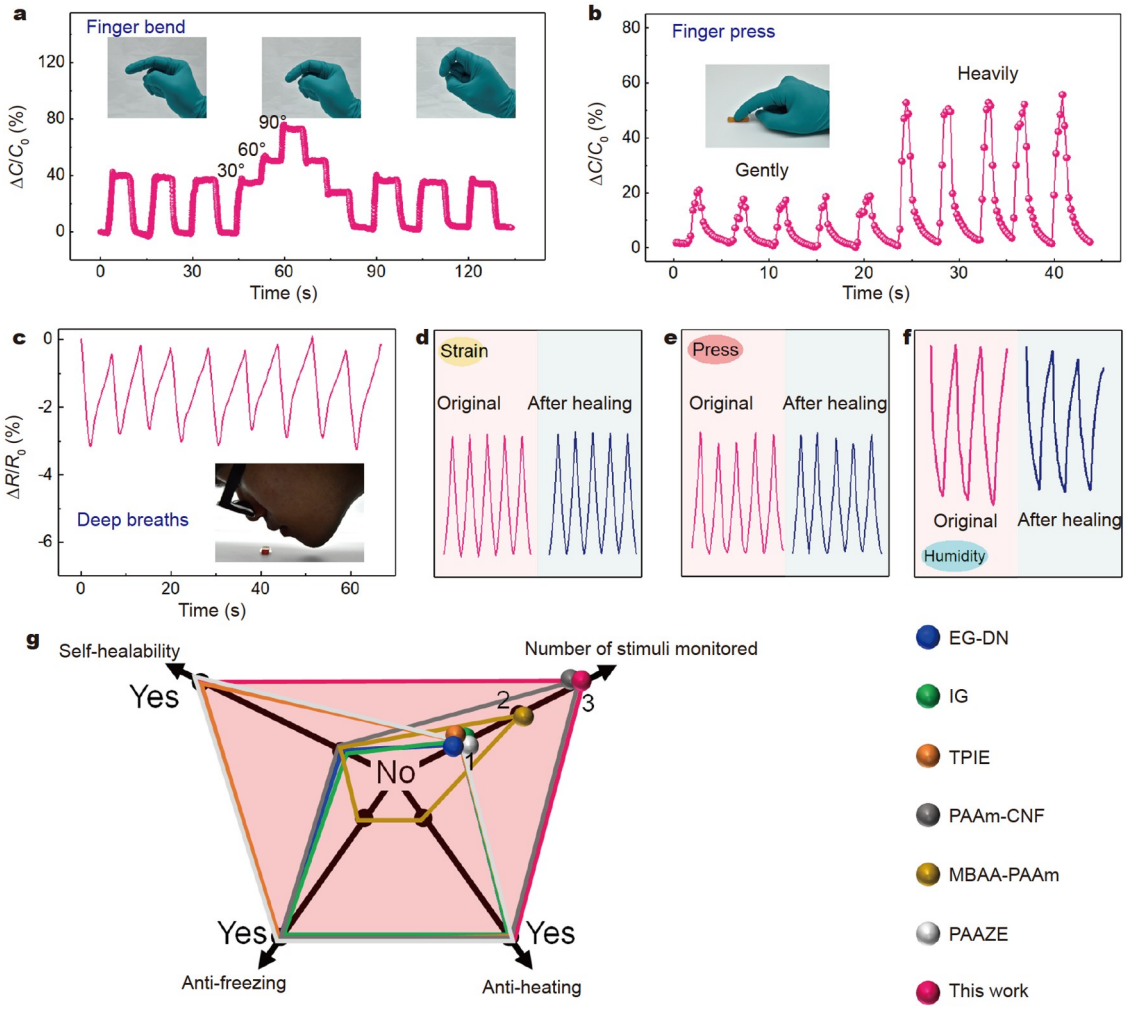

Figure 6 Self-healable PAIFe-2 skin-inspired sensor detecting complex biomedical signals. Relative capacitance variations of the PAIFe-2 sensor in response to (a) finger bending, (b) pressing by finger and (c) deep breathing. Insets in (a–c) showing digital photographs of the finger bending, the pressing by finger and the deep breathing, respectively. Original and healed PAIFe-2 sensor detecting various kinds of stimuli of (d) strain, (e) pressure and (f) humidity. (g) Comparison of the PAIFe and other ionogels in the literature in terms of self-healability, anti-freezing property, anti-heating property and the number of detectable stimuli.

results suggest that the PAIFe-2 sensor can monitor various kinds of stimuli, which is of great significance to mimick the multifunctional human skin.

The self-healing ability improves the reliability, lifetime and safety of the devices. Fig. 6d–f show that the PAIFe-2 sensor exhibits a comprehensive range of self-healing properties, including strain, pressure, and humidity. When two pieces of fractured PAIFe-2 are healed into one piece, the device responds well to the external stimuli (stretching, compression, and moisture) and displays electrical signals similar to the initial state. The intriguing properties of the PAIFe-2 sensor with excellent temperature tolerance, self-healing ability and multimodal detection are greatly competitive compared with the previously reported skin-inspired sensors (Fig. 6g) [2,8,16,34,40,41]. Thus, the PAIFe-2 skin-inspired sensor has great prospects in multifunctional I-skin.

CONCLUSIONS

This study has developed a stretchable and self-healable ionogel (PAIFe) *via* a dynamic ionic cross-linking strategy. The fabrication of PAIFe using the [BMIm][BF_4] as a solvent not only greatly improves the temperature tolerance, but also achieves high ionic conductivity. More importantly, the unique hygroscopic property of the [BMIm][BF_4] is capable of tailoring the water contents in the PAIFe spontaneously according to the humidity changes in the air, which enables the PAIFe possible to detect the environmental humidity. The physically cross-linked structure of ionic coordination interactions enables the PAIFe to have a favorable self-healability, and it still shows a reliable healing efficiency (87%) even at a low temperature of −20°C. With the combined intriguing properties of stretchability, self-healability and hygroscopicity, the PAIFe-2 is a promising candidate for a multifunctional skin-inspired sensor. As a proof-of-concept, the multifunctional monitoring system based on the PAIFe-2 achieves a variety of sensory capabilities towards humidity, compression and strain. The device also exhibits a comprehensive range of self-healing properties, which improves the reliability and lifetime of the devices. Overall, the PAIFe

plays a vital role in the new-generation skin-inspired sensors, showing significant advantages of multimodal detection, excellent temperature tolerance and reliable self-healing performance.

Received 7 December 2021; accepted 24 January 2022; published online 14 March 2022

1 Wang M, Luo Y, Wang T, *et al.* Artificial skin perception. Adv Mater, 2021, 33: 2003014
2 Cao Z, Liu H, Jiang L. Transparent, mechanically robust, and ultrastable ionogels enabled by hydrogen bonding between elastomers and ionic liquids. Mater Horiz, 2020, 7: 912–918
3 Liu H, Zhang H, Han W, *et al.* 3D printed flexible strain sensors: From printing to devices and signals. Adv Mater, 2021, 33: 2004782
4 Niu S, Matsuhisa N, Beker L, *et al.* A wireless body area sensor network based on stretchable passive tags. Nat Electron, 2019, 2: 361–368
5 Gao Y, Wang Y, Xia S, *et al.* An environment-stable hydrogel with skin-matchable performance for human-machine interface. Sci China Mater, 2021, 64: 2313–2324
6 Yu HC, Zheng SY, Fang L, *et al.* Reversibly transforming a highly swollen polyelectrolyte hydrogel to an extremely tough one and its application as a tubular grasper. Adv Mater, 2020, 32: 2005171
7 Ren Y, Liu Z, Jin G, *et al.* Electric-field-induced gradient ionogels for highly sensitive, broad-range-response, and freeze/heat-resistant ionic fingers. Adv Mater, 2021, 33: 2008486
8 Bai J, Wang R, Ju M, *et al.* Facile preparation and high performance of wearable strain sensors based on ionically cross-linked composite hydrogels. Sci China Mater, 2021, 64: 942–952
9 Du W, Zhang J, Zhao Z, *et al.* Preparation of novel temperature-responsive double-network hydrogel reinforced with aramid nanofibers. Compos Commun, 2020, 22: 100438
10 Hao XP, Li CY, Zhang CW, *et al.* Self-shaping soft electronics based on patterned hydrogel with stencil-printed liquid metal. Adv Funct Mater, 2021, 31: 2105481
11 Lei W, Qi S, Rong Q, *et al.* Diffusion-freezing-induced microphase separation for constructing large-area multiscale structures on hydrogel surfaces. Adv Mater, 2019, 31: 1808217
12 Kim HJ, Paquin L, Barney CW, *et al.* Low-voltage reversible electroadhesion of ionoelastomer junctions. Adv Mater, 2020, 32: 2000600
13 Zhang H, Cong Y, Osi AR, *et al.* Direct 3D printed biomimetic scaffolds based on hydrogel microparticles for cell spheroid growth. Adv Funct Mater, 2020, 30: 1910573
14 Pan L, Wang F, Cheng Y, *et al.* A supertough electro-tendon based on spider silk composites. Nat Commun, 2020, 11: 1332
15 Mao J, Zhao C, Li Y, *et al.* Highly stretchable, self-healing, and strain-sensitive based on double-crosslinked nanocomposite hydrogel. Compos Commun, 2020, 17: 22–27
16 Zhang W, Wu B, Sun S, *et al.* Skin-like mechanoresponsive self-healing ionic elastomer from supramolecular zwitterionic network. Nat Commun, 2021, 12: 4082
17 Guo Y, Bae J, Fang Z, *et al.* Hydrogels and hydrogel-derived materials for energy and water sustainability. Chem Rev, 2020, 120: 7642–7707
18 Zhou X, Guo Y, Zhao F, *et al.* Topology-controlled hydration of polymer network in hydrogels for solar-driven wastewater treatment. Adv Mater, 2020, 32: 2007012
19 Lei Z, Wu P. A highly transparent and ultra-stretchable conductor with stable conductivity during large deformation. Nat Commun, 2019, 10: 3429
20 Ren Y, Guo J, Liu Z, *et al.* Ionic liquid-based click-ionogels. Sci Adv, 2019, 5: eaax0648
21 Li T, Wang Y, Li S, *et al.* Mechanically robust, elastic, and healable ionogels for highly sensitive ultra-durable ionic skins. Adv Mater, 2020, 32: 2002706
22 Chang L, Song M, Zhang J, *et al.* Tunable ionic liquid-water separation enabled by bioinspired superwetting porous gel membranes. ACS Appl Mater Interfaces, 2019, 11: 44844–44850
23 Yiming B, Guo X, Ali N, *et al.* Ambiently and mechanically stable ionogels for soft ionotronics. Adv Funct Mater, 2021, 31: 2102773
24 Matsuda T, Nakajima T, Gong JP. Fabrication of tough and stretchable hybrid double-network elastomers using ionic dissociation of polyelectrolyte in nonaqueous media. Chem Mater, 2019, 31: 3766–3776
25 Zhao X, Chen F, Li Y, *et al.* Bioinspired ultra-stretchable and anti-freezing conductive hydrogel fibers with ordered and reversible polymer chain alignment. Nat Commun, 2018, 9: 3579
26 Zhang B, Zhang X, Wan K, *et al.* Dense hydrogen-bonding network boosts ionic conductive hydrogels with extremely high toughness, rapid self-recovery, and autonomous adhesion for human-motion detection. Research, 2021, 2021: 1–14
27 Ding Y, Zhang J, Chang L, *et al.* Preparation of high-performance ionogels with excellent transparency, good mechanical strength, and high conductivity. Adv Mater, 2017, 29: 1704253
28 Ho DH, Sun Q, Kim SY, *et al.* Stretchable and multimodal all graphene electronic skin. Adv Mater, 2016, 28: 2601–2608
29 Du G, Mao A, Yu J, *et al.* Nacre-mimetic composite with intrinsic self-healing and shape-programming capability. Nat Commun, 2019, 10: 800
30 Zhang Q, Deng YX, Luo HX, *et al.* Assembling a natural small molecule into a supramolecular network with high structural order and dynamic functions. J Am Chem Soc, 2019, 141: 12804–12814
31 Li Z, Zhu YL, Niu W, *et al.* Healable and recyclable elastomers with record-high mechanical robustness, unprecedented crack tolerance, and superhigh elastic restorability. Adv Mater, 2021, 33: 2101498
32 Wu X, Luo R, Li Z, *et al.* Readily self-healing polymers at subzero temperature enabled by dual cooperative crosslink strategy for smart paint. Chem Eng J, 2020, 398: 125593
33 Wang Y, Tebyetekerwa M, Liu Y, *et al.* Extremely stretchable and healable ionic conductive hydrogels fabricated by surface competitive coordination for human-motion detection. Chem Eng J, 2021, 420: 127637
34 Wu J, Wu Z, Xu H, *et al.* An intrinsically stretchable humidity sensor based on anti-drying, self-healing and transparent organohydrogels. Mater Horiz, 2019, 6: 595–603
35 Zheng N, Xu Y, Zhao Q, *et al.* Dynamic covalent polymer networks: A molecular platform for designing functions beyond chemical recycling and self-healing. Chem Rev, 2021, 121: 1716–1745
36 Fan C, Wang D, Huang J, *et al.* A highly sensitive epidermal sensor based on triple-bonded hydrogels for strain/pressure sensing. Compos Commun, 2021, 28: 100951
37 Yu X, Wang Y, Zhang H, *et al.* Ultrastretchable and stable conductive elastomer based on micro-ionicgel for wide-working-range sensors. ACS Appl Mater Interfaces, 2021, 13: 53091–53098
38 Zhu T, Feng Q, Liu S, *et al.* Metallogel-derived 3D porous carbon nanosheet composites as an electrocatalyst for oxygen reduction reaction. Compos Commun, 2020, 20: 100376
39 Shi P, Wang Y, Tjiu WW, *et al.* Highly stretchable, fast self-healing, and waterproof fluorinated copolymer ionogels with selectively enriched ionic liquids for human-motion detection. ACS Appl Mater Interfaces, 2021, 13: 49358–49368
40 Wang Y, Liu Y, Plamthottam R, *et al.* Highly stretchable and reconfigurable ionogels with unprecedented thermoplasticity and ultrafast self-healability enabled by gradient-responsive networks. Macromolecules, 2021, 54: 3832–3844
41 Wei Y, Xiang L, Zhu P, *et al.* Multifunctional organohydrogel-based ionic skin for capacitance and temperature sensing toward intelligent skin-like devices. Chem Mater, 2021, 33: 8623–8634

Acknowledgements This work was financially supported by the National Natural Science Foundation of China (21875033 and 52122303).

Author contributions Wang Y, Zhang C and Liu T designed and performed the experiments and analyzed the data. Wang Y and Zhang C conceived the work and co-wrote the manuscript. Liu Y assisted with the strain, pressure and humidity sensing measurements. Hu N and Shi P assisted with the self-healing measurements. All authors have given approval to the final version of the manuscript.

Conflict of interest The authors declare that they have no conflict of interest.

Supplementary information Supporting data are available in the online version of the paper.

Yufeng Wang is a PhD student at the College of Materials Science and Engineering, Donghua University. He joined Prof. Tianxi Liu's group in 2017 and his research interest focuses on hydrogel and ionogel materials for ionic sensor and thermal management.

Chao Zhang is a professor at the College of Materials Science and Engineering, Donghua University. He received his PhD degree from Fudan University in 2013. His research interests include ionic conducting elastomers for wearable sensors, and photothermal-regulated aerogels for thermal management.

Tianxi Liu obtained his BSc degree from Henan University (1992) and PhD degree from Changchun Institute of Applied Chemistry, Chinese Academy of Sciences (1998). He is currently a full professor at the College of Materials Science and Engineering, Donghua University. His main research interests include polymer nanocomposites, organic/inorganic hybrid materials, nanofibers and their composites, and advanced energy materials for energy conversion and storage.

高可拉伸、可自修复和湿度敏感的离子凝胶用于多模式感知的类皮肤传感器

王煜烽[1], 刘颖[1], 胡楠[1], 史佩茹[1], 张超[1*], 刘天西[1,2*]

摘要 离子皮肤(I-skin)作为一类新兴的类皮肤传感器，在下一代可穿戴电子领域受到了越来越多的关注. 然而, I-skin在实现多重刺激响应(如应变、压力和湿度等)和模仿皮肤的自修复功能等方面, 仍然面临着大的挑战. 本文通过动态离子交联策略, 制备了具有高可拉伸、耐极端温度和可自修复的Fe^{3+}离子配位聚丙烯酸离子凝胶(PAIFe). PAIFe中高度动态的离子配位作用和氢键交联结构, 使离子凝胶即使在−20°C低温条件下仍具有高效的自修复性能. 1-丁基-3-甲基咪唑四氟硼酸盐([BMIm][BF_4])作为离子凝胶的分散介质，赋予了PAIFe良好的抗冻/耐热性能. 更有趣的是，通过巧妙地利用[BMIm][BF_4]的吸湿特性，实现了PAIFe对环境湿度的传感功能. 作为概念性验证, PAIFe作为可拉伸离子导体可组装成多模式感知的类皮肤传感器，在湿度、压缩和应变的不同外界刺激下表现出良好的响应能力.

